This is a pre-copy-editing, author-produced PDF of an article accepted for publication in **"Glycobiology"** following peer review.

The definitive publisher-authenticated version:

High-resolution longitudinal N- and O-glycoprofiling of human monocyte-to-macrophage transition.

Hannes Hinneburg, Jessica L Pedersen, Nilesh J Bokil, Alexander Pralow, Falko Schirmeister, Rebeca Kawahara, Erdmann Rapp, Bernadette M Saunders, Morten Thaysen-Andersen

The article is available online at:

https://academic.oup.com/glycob/article-abstract/30/9/679/5775598?redirectedFrom=fulltext

High-resolution longitudinal *N*- and *O*-glycoprofiling of human monocyte-to-macrophage transition

Hinneburg, H.[1,2]; Pedersen, J.L.[3]; Bokil, N.J.[3]; Pralow, A.[4]; Schirmeister, F.; Kawahara, R.[1,2]; Rapp, E.[4, 5]; Saunders, B.M.[3]; Thaysen-Andersen, M.[1,2]*

[1]*Department of Molecular Sciences, Macquarie University, Sydney, Australia*

[2]*Biomolecular Discovery and Design Research Centre, Macquarie University, Sydney, Australia*

[3]*Faculty of Science, University of Technology Sydney, Australia*

[4]*Max Planck Institute for Dynamics of Complex Technical Systems, Magdeburg, Germany*

[5]*GlyXera GmbH, Magdeburg, Germany*

*Corresponding author:

Dr Morten Thaysen-Andersen

Macquarie University

NSW-2109, North Ryde

Sydney, Australia

Email: morten.andersen@mq.edu.au

Phone/Fax: +61 2 9850 7487/+61 2 9850 6192

Running title: Longitudinal *N*- and *O*-glycoprofiling of maturing macrophages

Abstract

Protein glycosylation impacts the development and function of innate immune cells. The glyco-phenotypes and the glycan remodelling associated with the maturation of macrophages from monocytic precursor populations remain incompletely described. Herein, label-free PGC-LC-MS/MS was employed to profile with high resolution the N- and O-glycome associated with human monocyte-to-macrophage transition. Primary blood-derived CD14$^+$-monocytes were differentiated *ex vivo* in the absence of strong anti- and pro-inflammatory stimuli using a conventional seven-day granulocyte-macrophage colony-stimulating factor differentiation protocol with longitudinal sampling. Morphology and protein expression monitored by light microscopy and proteomics validated the maturation process. Glycomics demonstrated that monocytes and macrophages display similar N-glycome profiles, comprising predominantly paucimannosidic (Man$_{1-3}$GlcNAc$_2$Fuc$_{0-1}$, 22.1%-30.8%), oligomannosidic (Man$_{5-9}$GlcNAc$_2$, 29.8%-35.7%) and α2,3/6-sialylated complex-type N-glycans with variable core fucosylation (27.6%-39.1%). Glycopeptide analysis validated conjugation of these glycans to human proteins while quantitative proteomics monitored the glyco-enzyme expression levels during macrophage differentiation. Significant inter-person glycome variations were observed suggesting a considerable physiology-dependent or heritable heterogeneity of CD14$^+$-monocytes. Only few N-glycome changes correlated with the monocyte-to-macrophage transition across donors including decreased core fucosylation and reduced expression of mannose-terminating (paucimannosidic-/oligomannosidic-type) N-glycans in macrophages, while lectin flow cytometry indicated that more dramatic cell surface glycan remodelling occurs during maturation. The less-heterogeneous core 1-rich O-glycome showed a minor decrease in core 2-type O-glycosylation, but otherwise remained unchanged with macrophage maturation. This high-resolution glycome map underpinning normal monocyte-to-macrophage transition, the most detailed to date, aids our understanding of the molecular makeup pertaining to two vital innate immune cell types and forms an important reference for future glycoimmunological studies.

Introduction

Complex carbohydrates (hereafter glycans) decorate and modulate the function of intra- and extracellular proteins in all eukaryotic species (Moremen, K.W., Tiemeyer, M., et al. 2012, Varki, A. 2016). Glycoproteins are secondary gene products; while their polypeptide sequences can be predicted from the coding genes, this is not the case for the conjugated glycans that are produced by template-less pathways. In human and other mammals, glycoprotein biosynthesis entails a complex series of enzymatic processing steps involving timely interactions of nascent glycoproteins with the many glycoside hydrolases and glycosyltransferases residing in the secretory machinery (Aebi, M. 2013). As a result, glycoproteins often display glycosylation signatures that accurately reflect the physiological state of the producing cell at the time of expression.

This complex and dynamic biosynthesis makes glycoproteins ideal to relay chemical information within and between cells and tissues; transmittable information that is tuneable to allow cells to aptly respond to physiological, pathological and ecological cues. Hence, it is not surprising that glycoproteins are involved in a broad array of biological processes including cell proliferation, adhesion, differentiation and signalling, processes that are known to be vital for the human immune system (Lau, K.S., Partridge, E.A., et al. 2007, Lyons, J.J., Milner, J.D., et al. 2015, Ohtsubo, K. and Marth, J.D. 2006, Springer, S.A. and Gagneux, P. 2016). For example, protein glycans are recognised to facilitate communication between and within the innate and adaptive immune system by modulating the thresholds for receptor activation (Cerliani, J.P., Blidner, A.G., et al. 2017, Clark, M.C. and Baum, L.G. 2012, van Kooyk, Y. and Rabinovich, G.A. 2008), and are key molecules involved in pathogen recognition mediated by antigen presenting cells such as dendritic cells and macrophages (van Kooyk, Y. and Rabinovich, G.A. 2008).

Surveillance of and response to microbial invasion by the innate immune system are processes contingent on a timely differentiation of circulating monocytes to more specialised effector cells including macrophages that are involved in tissue sensing, mobilisation of the adaptive immune response, and, ultimately, pathogen clearance (Gonzalez-Mejia, M.E. and Doseff, A.I. 2009). The bone

marrow-derived monocytes form an abundant population of mononuclear phagocytes in circulation. Monocytes are now recognised to carry out complex and diverse roles including phagocytosis and antigen presentation in circulation and in peripheral tissues and lymphoid organs (Jakubzick, C.V., Randolph, G.J., et al. 2017). These functions add important nuances to the more classical view that monocytes also form an important reservoir of precursor cells that differentiate into various types of macrophages and dendritic cells upon appropriate chemical stimulation. The monocyte-derived macrophages, the focus of this study, are considered distinctly different from the embryonically-derived self-replenishing macrophages residing in the peripheral tissues e.g. microglia in the brain, Kupffer cells in the liver and alveolar macrophages in the lung (Jakubzick, C.V., Randolph, G.J., et al. 2017). Due to their diverse origins and tissue residence, macrophages form a highly heterogeneous and dynamic population of powerful effector cells of the innate immune system involved in pathogen elimination, embryonic development and tissue repair via multiple mechanisms e.g. phagocytosis and antigen presentation (Hirayama, D., Iida, T., et al. 2017, Italiani, P. and Boraschi, D. 2014).

Both monocytes and macrophages express a spectrum of carbohydrate-recognising receptors that are known to be involved in phagocytosis of cells or, in the case of microbial pathogens, entire organisms, cellular debris or biomolecular complexes destined for phagocytosis by binding to terminal glycoepitopes presented by proteins or lipids. For instance, linkage-specific mannosyl- (Man-) or *N*-acetylglucosaminyl- (GlcNAc-) containing glycoepitopes on certain pathogens e.g. *Mycobacterium tuberculosis* are known to induce their clearance via phagocytosis facilitated by dedicated endocytic receptors such as Toll-like receptors (TLRs) e.g. TLR2 and C-type lectin receptors e.g. the macrophage mannose receptor amongst many other lectin receptors expressed by macrophages (Queval, C.J., Brosch, R., et al. 2017). Macrophages are highly specialised and adapted to their immunological niche and adequately fine-tuned to react to environmental stimuli. This is facilitated by an array of cell surface-located sensing receptors that together with a diverse class of transmembrane glycoproteins, proteoglycans, glycosphingolipids and glycosaminoglycans form important components of the glycocalyx. A growing body of literature supports that glycan-binding proteins and glycosylated

proteins play important and highly diverse roles in the innate immune system (Bax, M., García-Vallejo, J.J., et al. 2007, Nonaka, M., Ma, B.Y., et al. 2008).

The monocyte-to-macrophage transition process involves a time-segregated differentiation phase and a subsequent polarisation/activation phase. Although community consensus is yet to be reached, the differentiation, which *ex vivo* takes 5-7 days, but presumably is significantly faster *in vivo*, is thought to be a definitive event whereas macrophage polarisation shows plasticity according to the array of context-dependent signals individual macrophages may sense and integrate (Italiani, P. and Boraschi, D. 2014). Herein, we specifically focused on detailing the molecular signatures associated with macrophage differentiation as opposed to the subsequent macrophage polarisation phase. The monocyte-derived macrophages are commonly grouped into different types and subtypes based on their polarisation status and phenotype; M1- (or "classically" activated) macrophages are present in inflammatory settings dominated by TLRs and interferon signalling. The activation of these "pro-inflammatory" macrophages may be triggered by strong stimulants including a combination of granulocyte-macrophage colony-stimulating factor (GM-CSF) and infectious pro-inflammatory agents such as pathogenic lipopolysaccharides. The M1-macrophages are crucial to fight intruding pathogens such as *M. tuberculosis* (Walters, S.B., Kieckbusch, J., et al. 2013). In contrast, M2a-c-macrophages (or "alternatively" activated macrophages) are found in settings dominated by a T_H2 (anti-inflammatory) response (Gleissner, C. 2012, Italiani, P. and Boraschi, D. 2014, Murray, P.J. 2017). The M1 and M2 activation phenotypes differ from the non-activated M0-macrophages in their response to certain stimuli (Tarique, A.A., Logan, J., et al. 2015).

Molecular-level characterisation of macrophage maturation has been a focus over the past decade using gene expression, proteomics and surface marker analyses (Court, M., Petre, G., et al. 2017, Eligini, S., Brioschi, M., et al. 2015, Geissmann, F., Manz, M.G., et al. 2010, Kraft-Terry, S.D. and Gendelman, H.E. 2011, Martinez, F.O., Gordon, S., et al. 2006, Martinez, F.O., Sica, A., et al. 2008, Murray, P.J. 2017, Sander, J., Schmidt, S.V., et al. 2017). These studies have provided important

insights into the regulation associated with macrophage differentiation and polarisation. Relative to the uncommitted M0 phenotype, M1-macrophages display an altered expression of prostaglandin G/H synthase 2, tumour necrosis factor alpha, apolipoprotein L3, C-X-C motif chemokine 11, and interferon regulatory factor 5 (Mills, C.D., Kincaid, K., et al. 2000, Murray, P.J. 2017, Tarique, A.A., Logan, J., et al. 2015). Functionally-relevant alterations in protein glycosylation impacting the antigen receptor signalling and recognition events in the differentiation of human B cells and dendritic cells are also known to occur during immune cell differentiation (Bax, M., García-Vallejo, J.J., et al. 2007, Berger, R.P., Dookwah, M., et al. 2016, Giovannone, N., Antonopoulos, A., et al. 2018), and modulation of the expression levels and/or activity of several glycosylation enzymes i.e. glycosyltransferases and glycoside hydrolases during monocyte maturation into macrophages has repeatedly been reported (Delannoy, C.P., Rombouts, Y., et al. 2017, Kohro, T., Tanaka, T., et al. 2004, Trottein, F., Schaffer, L., et al. 2009). However, very limited biochemical literature is available to detail the actual protein glycosylation underpinning macrophage maturation (Delannoy, C.P., Rombouts, Y., et al. 2017, Zarif, J.C., Yang, W., et al. 2017), and a comprehensive time-resolved map of the *N*- and *O*-glycome signatures associated with monocyte differentiation to macrophages is still missing. To this end, we herein performed longitudinal whole cell *N*- and *O*-glycome profiling of the GM-CSF-induced transition of human CD14^{+}-monocytes into macrophages at high-definition by mass spectrometry-based glycomics and accompanying proteomics, glycopeptide analysis, microscopy and lectin flow cytometry to also monitor the cell surface glycan remodelling.

Material and Methods

The chemicals and reagents used in this study were of analytical-grade or higher and were, if not stated otherwise, obtained from Sigma-Aldrich/Merck KGaA, Darmstadt, Germany.

Source and isolation of human monocytes

Buffy coats from healthy de-identified donors were provided by the Australian Red Cross (Sydney, Australia) with approval from the UTS Human Research Ethics Committee, Ref # ETH 19-3807. The age, gender and other donor information were not disclosed by the provider of the donor specimens. Peripheral blood mononuclear cells were isolated over Ficoll-Paque, and monocytes were isolated to purity (typically >95%) using positive $CD14^+$ selection (Miltenyi Biotec, Sydney, Australia) as described (Walters, S.B., Kieckbusch, J., et al. 2013). Cells from a minimum of three different donors were used for all assays. $CD14^+$-monocyte isolation and differentiation were carried out multiple times to conduct the various assays.

Monocyte-to-macrophage differentiation

Isolated $CD14^+$-monocytes from three donors were resuspended in DMEM media (Thermo Fisher Scientific, Sydney Australia) supplemented with 10% foetal bovine serum (FBS), 100 U/mL penicillin, 100 µg/mL streptomycin and 10 ng/mL GM-CSF, plated in 12 well plates at 10^6 cells/well and cultured for up to seven days. Cells from the three donors were plated separately for each time point allowing for donor-specific longitudinal monitoring (paired data points). Monocyte differentiation was monitored daily using a wide field light microscope (EVOS FL, Thermo Fisher Scientific) at 10X, 20X and 40X magnification. Cells were harvested on day 0, 1, 3, 5 and 7 during differentiation after washing the adherent cells thoroughly with cold PBS. Cells were washed a further three times with PBS in attempts to remove all traces of any contaminating FBS, and finally resuspended in 500 µL PBS containing a cocktail of Pierce™ protease and phosphatase inhibitors (Thermo Scientific).

Lectin flow cytometry

The monocyte-macrophage cell populations were harvested in PBS and washed with Hank's balanced salt solution on day 0, 1, 3, 5 and 7 during monocyte differentiation. Changes in cell surface glycosylation were assessed using concanavalin A (ConA) CF™ 640R and wheat germ agglutinin (WGA) CF™ 405M (Biotium, Fremont, CA) as per the manufacturer's instructions. The surface expression of glycoepitopes was measured on a Beckman Coulter CytoFLEX LX flow cytometer (Indianapolis, USA). Data was analysed using the FlowJo v10 software (FlowJo LLC, USA).

Cell lysis and protein extraction

Harvested cell populations (monocytes and maturing or fully mature macrophages) from each of the three donors were lysed in technical triplicates at each time point in 500 µL PBS containing a cocktail of Pierce™ protease and phosphatase inhibitors (Thermo Scientific) with sonication using a Branson 450 Digital Sonifier for 5-10 s at 38% output level on ice. Homogeneous cell lysates were obtained by adding 2% (w/v) sodium dodecyl sulfate (final concentration) to the samples which were then centrifuged for 20 min at 2,000g at 4°C. The supernatants containing the protein extracts of interest were transferred to new tubes for glycomics and proteomics analyses. While the protein extracts from all samples were profiled using glycomics, the technical replicates obtained at each time point were combined for quantitative proteomics and glycopeptide analysis.

N- and O-glycan release and sample preparation

Protein extracts (20 µg) were spotted onto an activated PVDF membrane, dried, stained and the *N*- and *O*-glycans sequentially released and processed as previously described (Jensen, P.H., Karlsson, N.G., et al. 2012). In short, the *N*-glycans were released using 10 U (1 µL) peptide:*N*-glycosidase F (Promega, Madison, WI) in PBS overnight at 37°C. The *N*-glycans were then reduced using 1 M sodium borohydride (final concentration) at 50°C, 3 h and desalted using a dual solid-phase extraction (SPE) procedure comprising sequential strong cation exchange-C_{18}-SPE and Hypercarb-SPE. The *N*-glycans were dried and dissolved in 10 µL MilliQ water.

The *O*-glycans were subsequently released from the same protein spots by overnight incubation in 0.5 M sodium borohydride in 50 mM aqueous potassium hydroxide (final concentrations) at 50°C. The reduced *O*-glycans were desalted as described for *N*-glycans and dissolved in 10 µL MilliQ water. The *N*- and *O*-glycans were profiled separately using porous graphitised carbon (PGC) LC-MS/MS.

Protein denaturation and tryptic peptide generation

For label-free proteomics, the protein extracts were first processed using methanol-chloroform precipitation (Wessel, D. and Flugge, U.I. 1984). The pellet was dissolved in 4 M urea in 50 mM triethylammonium bicarbonate (TEAB) (pH 8.5). Proteins were reduced and alkylated by the addition of 10 mM dithiothreitol (37°C, 30 min), 40 mM iodoacetamide (room temperature, 30 min in the dark), and then 20 mM dithiothreitol to quench the alkylation reaction (all final concentrations). Samples were diluted with 50 mM TEAB to reach concentrations below 1 M urea. Sequencing grade trypsin (Promega) was added in a 1:30 (w/w, enzyme/protein) ratio. Samples were incubated overnight at 37°C and the reactions were stopped by acidification using trifluoroacetic acid. Peptides were desalted using Oligo R3-SPE clean up prior to proteomics (PerSeptive Biosystems, Framingham, MA).

LC-MS/MS parameters, data analysis and statistics for glycomics profiling

Glycomics profiling of both the *N*- and *O*-glycome was performed using our recently described PGC-LC-MS/MS platform employing a post-column-makeup flow, which supplements methanol (57% v/v, final concentration) to the main LC solvents (Hinneburg, H., Chatterjee, S., et al. 2019). Briefly, glycans were separated on a capillary PGC-LC column (Hypercarb, 3 µm particle size, 180 µm I.D. x 100 mm, Thermo Scientific) heated to 50°C. For the *N*-glycan separation, the multi-step gradient made from 10 mM aqueous ammonium bicarbonate (solvent A) and 10 mM ammonium bicarbonate in 70% (v/v) acetonitrile (ACN, solvent B) was 2.6% (v/v) B for 8 min, a linear increase to 13.5% (v/v) B over 2 min, to 37.3% (v/v) B over 55 min, and to 64% (v/v) B over 10 min, before the column was cleaned in 98% (v/v) B for 6 min and equilibrated in 2.6% (v/v) B. A Dionex UltiMate 3000 LC system (Thermo Scientific)

was used to deliver a constant column flow rate of 3 µL/min. For the *O*-glycan analysis, the gradient was 2.8-30% (v/v) B over 38 min before a linear ramp to 98% (v/v) B over 5 min was applied, followed by a 2 min column clean in 98% (v/v) B and column re-equilibration in 2.8% (v/v) B.

A Velos linear ion trap (LTQ, Thermo Scientific) operating in negative ion polarity mode (HESI-II probe position B depth) was used for data acquisition with the following parameters: Capillary voltage of -2.7 kV, capillary heating to 275°C, 3 microscans, 5×10^4 automatic gain control (AGC) (zoom 3.7×10^4) and a maximum accumulation time of 100 ms/scan. Resonance-activation collision-induced dissociation (CID) MS/MS of the top five most abundant precursor ions in each MS1 full scan was performed (2×10^4 AGC, 250 ms maximum accumulation time/scan). An precursor isolation window of 1.5-2 Th for CID-MS/MS with a normalised collision energy of 33%, an activation Q of 0.250 and an activation time of 10 ms was used for fragmentation. Dynamic exclusion was enabled with repeat counts set at a maximum of 5, repeat duration at 15 s and exclusion duration at 30 s. All spectra were acquired in profile mode. The MS1 spectra for the *N*-glycans were recorded in the range *m/z* 570–2,000 while the smaller *O*-glycans were recorded using *m/z* 375-1,800.

Spectral annotation was performed manually using Xcalibur v2.2 (Thermo Scientific). All glycans were identified based on their monoisotopic mass, CID-MS/MS fragmentation pattern and the relative abundance of the fragment ions (Everest-Dass, A.V., Jin, D., et al. 2012, Harvey, D.J. 2005a, Harvey, D.J. 2005b, Thaysen-Andersen, M., Mysling, S., et al. 2009), and the relative and absolute PGC-LC retention time behaviour (Abrahams, J.L., Campbell, M.P., et al. 2018, Pabst, M. and Altmann, F. 2008, Palmisano, G., Larsen, M.R., et al. 2013). The observed glycans were further validated using knowledge of the human biosynthetic machinery and the expected structural relationships between the observed glycans (Trombetta, E.S. 2003, Varki A, C.R., Esko JD, et al., editors. 2015-2017). The latest symbol nomenclature was used for the graphical representations of the glycans (Varki, A., Cummings, R.D., et al. 2015). **Supplementary data 1** is a compilation of annotated fragment spectra of all reported glycans. For relative glycan quantitation, the area-under-the-curve of the monoisotopic peak of extracted ion chromatograms of all observed charge states of each identified glycan was determined

using Skyline (64-bit) v3.7.0.11317 (Ashwood, C., Lin, C.H., et al. 2018), see **Extended experimental section** for settings.

The quantitative glycan data was analysed and visualised using the language and environment for statistical computing R v3.4.2 (https://www.R-project.org/) and Microsoft Excel 2013, respectively. Data points have generally been plotted as the mean of technical and/or biological replicates as indicated for the individual experiments. Error bars indicate their standard deviation. The mean relative abundance values of *N*-glycans were plotted as a heat map using the R-package *pheatmap* v1.0.10. Paired, two-tailed Student's T-tests were used for statistical testing of the data; p-value correction for multiple testing was applied when appropriate according to Benjamini and Hochberg (Benjamini, Y.a.H., Y. 1995); $p < 0.05$ was used as the minimum significance threshold. For further details of the statistical testing, see SI. The R code is available upon request.

LC-MS/MS parameters, data analysis and statistics for proteomics and glycopeptide analysis

(Glyco-)peptides were analysed using nano-flow reversed-phase liquid chromatography using a Dionex UltiMate 3000 RSLCnano system (Thermo Scientific) coupled online to a Q Exactive HF-X Hybrid Quadrupole-Orbitrap mass spectrometer (Thermo Scientific). Peptides (1.5 µg) were loaded under isocratic conditions on a C18 nano-trap column (Halo-C18, 160 Å, 2.7 µm, 100 µm x 3.5 cm, Advanced Materials Technology, Wilmington, DE) using 0.1% (v/v) aqueous formic acid (FA) (solvent A) delivered by the loading pump at a flow rate of 5 µL/min. The C18 nano-scale pre-column cycle was connected after 5.9 min by a valve switch. The C18 nano-scale analytical column (Halo-C18, 160 Å, 2.7 µm, 100 µm x 30 cm) was heated to 45°C. Solvent B was 0.1% (v/v) FA in 99 % (v/v) ACN. A constant flow rate of 600 nL/min was used. The gradient was as follows: 6 min 2% (v/v) B, followed by an increase to 30% (v/v) B over 100 min, to 50% (v/v) B over 18 min, and a 1 min increase to 95% (v/v) B, which was held for 9 min before dropping to 2% (v/v) B over 1 min to re-equilibrate the column for 15 min. The total run time was 150 min. The pre-column and analytical column cycles were disconnected by a valve switch at 137 min.

The mass spectrometer was operated in positive ion mode. The source was equipped with stainless steel nano-bore emitters (Thermo Scientific). MS parameters were as follows: Source voltage (2.7 kV); capillary temperature (250°C); sheath gas flow, auxiliary gas flow, and sweep gas flow were set to zero. Full MS1 scan spectra were acquired between m/z 350-1,800 at a resolution of 60,000 using profile mode; the AGC target was set to 3×10^6; and maximum injection time was set to 50 ms. Fragment ion (MS/MS) spectra were obtained of the top 20 most intense precursor ions (charge state $Z \geq 2$ and signal intensity $\geq$ 10,000 AGC) by subjecting isolated precursors to higher-energy collisional dissociation (HCD). Resolution was set at 15,000, AGC at 2×10^5, the maximum injection time at 28 ms and fixed first mass at m/z 100. The normalised collision energy was set to 30. The precursor isolation window was 1.2 Th. Isotopes were excluded and dynamic exclusion was set to 30 s.

Label-free identification and quantitation was performed using MaxQuant v1.6.3.4 and statistical analysis using Perseus v1.6.2.2 (Cox, J. and Mann, M. 2008) by searching against the human proteome (20,404 reviewed entries; downloaded from UniProtKB on April 4, 2019) and bovine proteome (6,006 reviewed entries; downloaded April 18, 2019). Potential contaminants and decoy hits (known false positives) were excluded from the lists of reported proteins. Significant alterations in the protein expression were identified using one-way ANOVA (multiple sample testing) and a significance threshold of $p < 0.05$. Only significantly regulated proteins were used as input for the pathway analysis using DAVID v6.8 (Huang da, W., Sherman, B.T., et al. 2009). Pathways with Benjamini & Hochberg adjusted $p < 0.05$ and FDR < 0.05 were accepted as being significantly altered.

Intact glycopeptide analysis was performed manually using Xcalibur v2.2 (Thermo Scientific) with aid from Byonic v.2.16.11 (Protein Metrics Inc, Cupertino, CA) (Lee, L.Y., Moh, E.S., et al. 2016). In short, the following Byonic search parameters were used: The protease cleavage specificity was trypsin (fully specific) with a maximum of one missed cleavage, the precursor ion mass tolerance was 10 ppm, the fragment ion tolerance was 0.04 Da, carbamidomethylation of Cys was a fixed modification, and

oxidation of Met was a variable modification. The glycan search space used to identify intact *N*- and

O-glycopeptides was 310 pre-defined mammalian *N*-glycans and 78 *O*-glycans, respectively.

Results and Discussion

GM-CSF differentiation of human monocytes to macrophages is one of the most extensively used techniques to derive mature macrophages for biochemical and biomedical research. Given that in humans, tissue-derived macrophages are frequently not available, monocyte-derived macrophages represent an important tool for the analysis of macrophage function. These monocytes are commonly matured using the method described in this work and on day 6-7 stimulated with inflammatory stimuli such as LPS or infected with pathogens such as *M. tuberculosis*. While this model does not perfectly recapitulate the *in vivo* situation with tissue-resident macrophages or tissue inflammatory monocytes, it provides a context to investigate changes in these cells in response to specific stimuli that would otherwise not be available to researchers in most instances. Investigation and characterisation of the glycosylation changes that occur during conventional monocyte differentiation, in the absence of strong pro- or anti-inflammatory stimuli such as infection, was the aim of this study.

To this end, this study has generated the first high-definition longitudinal map of the protein *N-* and *O*-glycome associated with the maturation of human macrophages from healthy CD14$^+$-monocytic precursors. A conventional differentiation protocol used widely in immunobiology employing GM-CSF-mediated maturation of primary CD14$^+$-monocytes over seven days was used with longitudinal sampling at day 0, 1, 3, 5, and 7, **Figure 1A**. We used our recently improved label-free glycomics method employing post-column make-up flow in conjunction with PGC-LC-MS/MS operating in negative-ion mode to obtain quantitative fine structure information of the *N-* and *O*-glycome of maturing macrophages at high sensitivity with temporal resolution (Hinneburg, H., Chatterjee, S., et al. 2019). Label-free quantitative LC-MS/MS-based proteomics and glycopeptide analysis as well as lectin flow cytometry and microscopy provided additional molecular level and morphological information of the differentiation process.

Validation of the monocyte-to-macrophage transition by morphology and protein expression

The morphology of the CD14$^+$-monocyte population was monitored by light microscopy during differentiation, **Figure S1**. The maturing cells acquired adhesion properties by day 1. The transformation to a more heterogeneous and voluminous cell type with cellular extensions and irregular morphology was not observed until day 5. The characteristic pseudopodia-rich macrophage morphology indicating terminal macrophage maturation was observed from day 5 and 6, but not fully reached until day 7.

Quantitative proteomics confidently identified a total of 2,600 human proteins across the monocyte-macrophage development stages, **Table S1**. Functional annotation using DAVID identified a number of expected protein pathways including enriched pathways related to classical metabolic and immune processes such as signal transduction, redox processes, cell-cell adhesion, protein transport and innate immune/inflammatory responses, **Table S2** (Kraft-Terry, S.D. and Gendelman, H.E. 2011, Sander, J., Schmidt, S.V., et al. 2017). Despite rigorous washing of the *ex vivo* cultured cells prior to lysis and profiling, additional sets of proteins were detected including 1,140 proteins ambiguously assigned as either of human or bovine origin and 101 proteins arising unambiguously from a bovine source, **Table S3-S4**. The bovine protein interference, which possibly originated from the FBS, a critical culture medium component for the *ex vivo* differentiation protocol, was assessed by protein intensity to be of lower abundance than the detected human proteins, and was found to remain constant over the differentiation process, as shown for three abundant bovine proteins i.e. bovine pancreatic trypsin inhibitor, bovine F-actin-capping protein subunit beta and bovine fetuin, **Figure S2** and **Table S5-S6**. The bovine FBS interference, which may have contributed to, but not longitudinally skewed, the glycome profiles reported herein, may be a functional, yet still unwanted consequence, of the phagocytotic nature of monocytes and macrophages.

Since the aim of the proteome profiling was to validate the monocyte-to-macrophage transition rather than to map the deep proteome of monocyte-macrophage populations (Kraft-Terry, S.D. and Gendelman, H.E. 2011), we decided to only use the identified proteins that unambiguously could be

confirmed to originate from a human source for the functional analysis and for the subsequent exploration of the monocyte-macrophage glycoproteome.

Unsupervised hierarchical clustering of a subset of 124 proteins identified as being differentially expressed across the monocyte-to-macrophage transition ($p < 0.05$, see **Table S7** for data and statistics) showed that the day 0-3 proteome expression was distinctly different from the day 5-7 proteome expression, **Figure S3**. The glycomics data to some extent recapitulated these early-to-late maturation stage differences (see below). Pathway analysis using the 124 differentially expressed proteins as input demonstrated that phagocytosis (17.2-fold enrichment, adjusted $p < 0.02$) and cell adhesion (7.5-fold enrichment, adjusted $p < 0.04$) were, as expected, significantly enriched biological processes associated with macrophage maturation, **Table S8-S10**.

Further, the proteomics data demonstrated a maturation stage-dependent expression of specific proteins previously associated with human monocytes and macrophages. For example, proteins known to be a molecular feature of monocytes were found to be down-regulated with progressive macrophage maturation including neutrophil elastase ($p = 0.0021$), cathepsin G ($p = 0.000097$) and myeloperoxidase ($p = 0.0043$) (Kargi, H.A., Campbell, E.J., et al. 1990, Khan, A.A., Alsahli, M.A., et al. 2018), while proteins known to be enriched in macrophages concomitantly displayed increased expression levels with progressive phagocyte maturation including apolipoprotein E ($p = 0.0032$, all two-tailed paired student's t-test, day 0 vs. day 7) (Tedla, N., Glaros, E.N., et al. 2004, Zhang, W.Y., Gaynor, P.M., et al. 1996), **Figure S4**. These expected expression patterns served to further validate the GM-CSF-based macrophage maturation.

Relevant to our observation, human M2-macrophages arising from *ex vivo* stimulation of primary monocytes with macrophage colony-stimulating factor were previously reported to undergo significant mid-stage (day 3 to day 5) proteome changes involving several altered biological processes i.e. cell-to-cell signalling/interaction, cellular function/maintenance, free radical scavenging, molecular transport and carbohydrate metabolism (Kraft-Terry, S.D. and Gendelman, H.E. 2011). The

observation of similar yet distinctly different proteome changes underpinning the functionally different M1- and M2-macrophages is not surprising giving their common progenitor and their *in vivo* plasticity and interchangeability (Italiani, P. and Boraschi, D. 2014).

Mannose- and sialic acid-rich N-glycosylation features of human CD14^{+}-monocytes and macrophages

Glycomics profiling revealed an extensive *N*-glycome heterogeneity of the studied monocyte-macrophage cell populations. In total, 102 *N*-glycans comprising many biosynthetically related isomers spanning 54 monosaccharide compositions were quantified, see **Supplementary data 1** for annotated fragment spectra of all reported glycans and **Table S11-S27** for other supporting glycomics data. The mannose-terminating glycans comprising both the common oligomannosidic (29.8%-35.7%) and the less reported paucimannosidic (22.1%-30.8%) *N*-glycan types were found to be consistently abundant across all samples, **Figure 1B**. In particular, M6-M9 ($Man_{6-9}GlcNAc_2$) and M2(F) ($Man_2GlcNAc_2Fuc_{0-1}$) were abundant *N*-glycan species. The distinct PGC-LC elution pattern and the informative negative polarity CID-MS/MS spectral evidence (see Supplementary data 1) as well as multiple observations at the glycopeptide level (see below), collectively confirmed that the less reported paucimannosidic *N*-glycans are not mass spectrometry artefacts. Instead, it is clear that this non-conventional glycan class is carried by human glycoproteins residing in intracellular compartments and are generate through an elaborate truncation pathway involving the action of *N*-acetyl-β-hexosaminidases and possibly linkage-specific α-mannosidases that is distinctly different from the conventional anabolic glycosylation machinery in the ER-Golgi-based secretory pathway (Tjondro, H.C., Loke, I., et al. 2019). These truncated glycoproteins are known to arise from highly processed glycoprotein intermediates generated by the action of GlcNAc-transferase I and in some cases fucosyltransferase VIII, but the timing and the cellular location of the final trimming events catalysed by these glycoside hydrolases and indeed the function of paucimannosidic proteins in monocytes and macrophages remain elusive. Further, the highly branched α2,3/6-sialylated complex-type *N*-glycans mostly comprising bi- and tri-antennary glycans variably decorated with α1,6-(core) fucosylation formed another abundant *N*-

glycan type within the monocyte-macrophage *N*-glycome (27.6%-39.1%). For the sialylated *N*-glycans where the two prominent sialyl-linkage types (α2,3- or α2,6-) could confidently be assigned (the case for all mono- and bi-antennary *N*-glycans), the longitudinal *N*-glycome profiling demonstrated that α2,6-sialylation (8.0%-10.4%) consistently was higher than the α2,3-sialylation (2.4%-3.5%). The quantitative glycomics data also showed that the relative expression levels of these two sialyl-linkage isomers remained unchanged over the maturation course, **Table S19**.

While PGC-LC-MS/MS is a recognised gold standard to obtain quantitative glycomics data with fine structure resolution, a method used by many laboratories world-wide (Chatterjee, S., Lee, L.Y., et al. 2019), the approach has limitations that are important to point out. Similar to other glycoanalytical techniques, PGC-LC-MS/MS often leaves some structural ambiguity of the identified glycans, particularly of the glycosidic linkage types and branch points of larger complex glycans that typically exist as many glycan isomers with identical masses. Another shortcoming is that the biosynthetically "extreme" glycans, for example, the highly truncated chitobiose core-type *N*-glycans only containing one or few monosaccharide residues of low molecular mass or very large, branched, and/or acidic glycans may go undetected in PGC-LC-MS/MS glycomics experiments due to poor or irreversible PGC-LC retention and due to limitations in the detection of such analytes that may be outside the optimal *m/z* detection window of the mass spectrometer (Abrahams, J.L., Packer, N.H., et al. 2015). Indeed, such difficult-to-study *N*-glycans including glycans displaying poly-*N*-acetyllactosamine extensions and highly branched sialyl Lewis-type structures may functionally be involved in or simply passively mark the monocyte differentiation process and should thus be explored in the context of monocyte-macrophage maturation once the available technologies allow for their accurate profiling.

Supporting our *N*-glycome profiling data, Delannoy and colleagues previously used MALDI-TOF-MS/MS profiling of permethylated glycans to demonstrate that undifferentiated monocytic THP-1 cells (resembling our CD14⁺-monocytes at day 0) abundantly express oligomannosidic-type *N*-glycans and highly branched sialylated complex-type *N*-glycans carrying core and antenna fucosylation

(Delannoy, C.P., Rombouts, Y., et al. 2017). We identified 28 of the 40 structures (70.0%) reported in their study, **Table 1**. The paucimannosidic-type *N*-glycans were, however, not reported in their study possibly due to the chosen analytical strategy, which may have precluded the detection of the low-mass glycans.
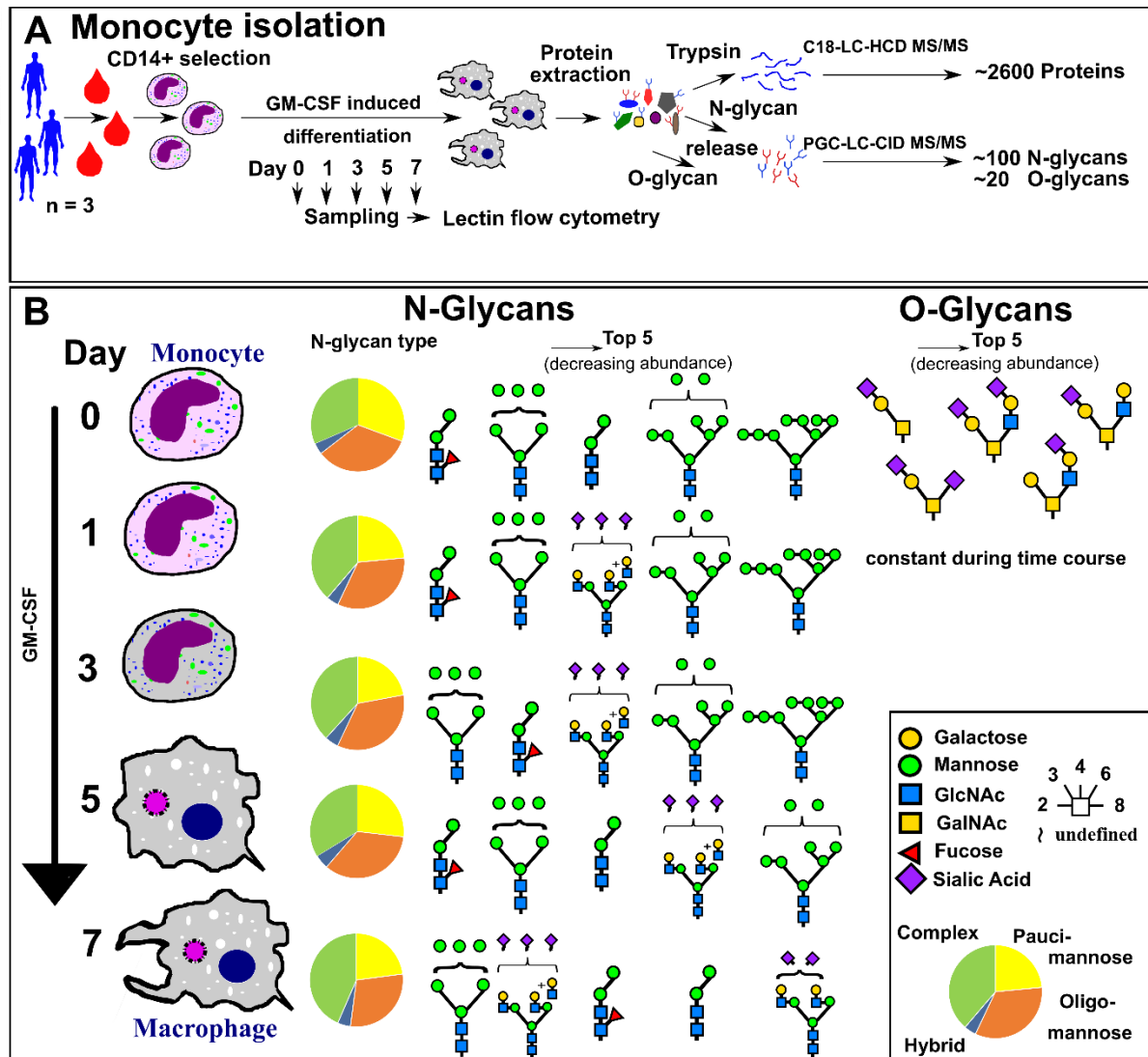

Figure 1. **High-resolution *N*- and *O*-glycome map of maturing macrophages using quantitative glycomics. A**) Overview of the experimental design used to generate a longitudinal map of the protein *N*- and *O*-glycome associated with GM-CSF-mediated monocyte-to-macrophage maturation over seven days from healthy donors using label-free quantitative glycomics and accompanying proteomics, glycopeptide analysis, microscopy and lectin flow cytometry. **B**) Overview of the longitudinal glycome data focusing on the abundantly expressed *N*- and *O*-glycans over the five sampling points. See insert for key.

In another related study, we recently characterised the *N*-glycome of phorbol 12-myristate 13-acetate-differentiated THP-1 cells (resembling the day 7 macrophages of this study) using PGC-LC-MS/MS (Hare, N.J., Lee, L.Y., et al. 2017). The high abundance of oligomannosidic- (~40%) and paucimannosidic (~50%) *N*-glycan types as well as complex-type tri- and tetra-antennary sialoglycans with variable core fucosylation (~10%) of differentiated THP-1 cells agreed well with the macrophage *N*-glycome phenotype reported herein. In fact, the same 18 *N*-glycans were reported by both studies, but notably a much greater coverage of the *N*-glycome was achieved in this study (64 vs. 18 compositions) as a likely result of the improved sensitivity of the employed glycome profiling strategy (Hinneburg, H., Chatterjee, S., et al. 2019).

Finally, Bax and colleagues (Bax, M., García-Vallejo, J.J., et al. 2007) used MALDI-TOF-MS/MS to profile permethylated *N*-glycans of blood-derived CD14$^+$-monocytes supplemented with GM-CSF (corresponding to day 5 cells of this study). The authors reported a profile dominated by oligomannosidic- and highly branched complex-type sialo-*N*-glycans. We identified 23 of the 48 structures (47.9%) reported in their study, which also underestimated the presence of the paucimannosidic-type glycans relative to our PGC-LC-MS/MS-based profiling. Taken together, this literature comparison adds confidence to our *N*-glycome data and demonstrates that our high-definition longitudinal whole cell glycome map obtained from maturing primary cell populations has expanded the coverage of the monocyte-macrophage *N*-glycome.

Table 1. Comparison of the *N*-glycans observed in this study to the monosaccharide compositions reported in three related glycomics studies of primary and THP-1 monocyte-macrophage populations (Bax, M., García-Vallejo, J.J., et al. 2007, Delannoy, C.P., Rombouts, Y., et al. 2017, Hare, N.J., Lee, L.Y., et al. 2017). xxxx, single most abundant *N*-glycan composition; xxx, top 2-5; xx, top 6-10; x, identified and quantified glycan composition of relatively low abundance; (x), identified, but not quantified glycan detected at trace levels. #No quantitative data available *Ethyl-esterified *N*-glycans (MS intensities, only top 6). *Italics*, not detected in this study. Please note that the glycan fine structures have been elucidated for all monosaccharide compositions reported in this study, see **Table S11**.

N-glycan type / monosaccharide composition	This study	Hare et al. 2017	Delannoy et al. 2017*	Bax et al. 2007#
Cell population studied	CD14+ Mono / Mac	Diff. THP-1	Diff THP-1	CD14+ Mono / DCs
Paucimannosidic-type N-glycans				
HexNAc2dHex1	x			
Hex1HexNAc2	x			
Hex1HexNAc2dHex1	x			
Hex2HexNAc2	xxx	xx		
Hex2HexNAc2dHex1	xxx	xxxx		
Hex3HexNAc2	xx	xxx		
Hex3HexNAc2dHex1	x	xxx		
Oligomannosidic-type N-glycans				
Hex4HexNAc2	x			
Hex5HexNAc2	xx	xx	xx	x
Hex6HexNAc2	xxx	xx	xxx	x
Hex7HexNAc2	xx	xx	xxx	x
Hex8HexNAc2	xx	xxx	xxx	x
Hex9HexNAc2	x	xxx	xxxx	x
Hex10HexNAc2	x	x	xxx	
Hybrid/complex-type N-glycans				
Hex5HexNAc3	x			
Hex6HexNAc3	x	x		x
Hex5HexNAc4	x	x		x
Hex5HexNAc3NeuAc1	x	x		
Hex6HexNAc3dHex1	x			
Hex5HexNAc3dHex1NeuAc1	x			
Hex6HexNAc3NeuAc1	x	x		
Hex7HexNAc3NeuAc1	x			
Hex4HexNAc4	x			
Hex4HexNAc5			x	
Hex3HexNAc3	x			
Hex3HexNAc3dHex1	x	x	x	
Hex4HexNAc3	x		x	
Hex3HexNAc4	(x)			
Hex4HexNAc3dHex1	x		x	
Hex3HexNAc4dHex1	x	x		
Hex3HexNAc5hex1	x		x	
Hex4HexNAc4dHex1	x			
Hex5HexNAc4dHex1	x	x	x	x
Hex5HexNAc4dHex2			x	
Hex5HexNAc4dHex3			x	x
Hex6HexNAc5	x		x	
Hex6HexNAc5dHex1	x		x	x
Hex7HexNAc6			x	
Hex7HexNAc6dHex1	x		x	x
Hex4HexNAc3NeuAc1	x			
Hex4HexNAc3dHex1NeuAc1	x			
Hex4HexNAc4NeuAc1	x			
Hex4HexNAc4dHex1NeuAc1	x			
Hex5HexNAc4NeuAc1	x		x	x
Hex5HexNAc4dHex1NeuAc1	x	xx	x	x
Hex5HexNAc4dHex2NeuAc1			x	x
Hex5HexNAc4dHex2NeuAc2			x	x
Hex5HexNAc4NeuAc2	xxx		x	x
Hex5HexNAc4dHex1NeuAc2	x		x	x
Hex5HexNAc4dHex3NeuAc2			x	
Hex5HexNAc4NeuAc3	(x)			
Hex5HexNAc4NeuAc3	(x)			
Hex6HexNAc5dHex2				x
Hex6HexNAc5NeuAc1	x		x	x
Hex6HexNAc5dHex1NeuAc1	x		x	x
Hex7HexNAc6NeuAc1	(x)		x	x
Hex7HexNAc6NeuAc2			x	x
Hex7HexNAc6NeuAc3			x	x
Hex7HexNAc6dHex1NeuAc1	(x)		x	x
Hex7HexNAc6dHex2				x
Hex7HexNAc6dHex3				x
Hex6HexNAc5NeuAc2	x		x	x
Hex6HexNAc5dHex2NeuAc1				x
Hex6HexNAc5dHex1NeuAc2	x		x	x
Hex6HexNAc5dHex2NeuAc2			x	
Hex6HexNAc5NeuAc3	xxxx		x	x
Hex6HexNAc6dHex1NeuAc3			x	
Hex6HexNAc6dHex1NeuAc1				x
Hex7HexNAc6dHex2NeuAc1				x
Hex7HexNAc6dHex1NeuAc2	x		x	x
Hex6HexNAc5NeuAc4	xx			
Hex7HexNAc6NeuAc4	(x)		x	x
Hex6HexNAc5dHex1NeuAc3	x			
Hex3HexNAc3NeuAc1	x			
Hex6HexNAc5NeuAc5	(x)			
Hex5HexNAc5NeuAc2	x			
unknown(1)	x			
unknown(2)	x			
Hex7HexNAc6dHex1NeuAc3	(x)		x	x
Hex7HexNAc6dHex1NeuAc4	(x)		x	
Hex8HexNAc7dHex1				x
Hex8HexNAc7NeuAc1				x
Hex8HexNAc7NeuAc2				x
Hex8HexNAc7NeuAc3				x
Hex8HexNAc7dHex1NeuAc1				x
Hex8HexNAc7dHex1NeuAc2				x
Hex8HexNAc7dHex1NeuAc3	(x)			x
Hex9HexNAc8NeuAc2				x
Hex9HexNAc8dHex1NeuAc1				x
Hex9HexNAc8dHex1NeuAc2				x
Hex9HexNAc8dHex1NeuAc3				x
Hex10HexNAc9NeuAc2				x
Hex12HexNAc11				x
Compositions identified	**64**	**18**	**40**	**48**
Glycans found in this study		**18**	**28**	**23**
Overlap with this study (%)		**100.0**	**70.0**	**47.9**

GM-CSF-mediated macrophage maturation induces only subtle whole cell N-glycome changes

The whole cell *N*-glycome expressed by CD14^{+}-monocytes and mature macrophages was found to be surprisingly similar as visually illustrated by a heat map plotting the relative *N*-glycan abundances over the differentiation course, **Figure 2A**. Only ten, seemingly biosynthetically unrelated, structures of a total of 102 *N*-glycans displayed a significantly altered expression over the maturation process including glycans belonging to the oligomannosidic-, hybrid-, and complex sialylated-type (all $p < 0.05$, two-tailed paired student's t-test, day 0 vs. day 7), **Table S12A**.

The *N*-glycan types were quantitatively monitored over the seven-day differentiation, **Figure 2B**(I-V). In concordance with a previous observation (Delannoy, C.P., Rombouts, Y., et al. 2017), the abundant mannose-terminating *N*-glycans (i.e. paucimannosidic- and oligomannosidic-type *N*-glycans) were reduced from 30.8% and 34.6% (day 0) to 23.1% and 29.8% (day 7), respectively, while the complex sialylated *N*-glycans concomitantly increased from 27.6% (day 0) to 39.1% (day 7), see **Table S13-S19**. None of these alterations, however, reached statistical significance possibly due to significant inter-donor variations within the population of isolated CD14^{+}-monocytes and in the subsequent differentiation process.

The distribution of the sialyl-linkage type (α2,3/6-) and the levels of core (α1,6-) fucosylation were also monitored. Only the expression of core fucosylated *N*-glycans was significantly altered in macrophages (20.1% ± 2.2%) relative to CD14^{+}-monocytes (31.5% ± 4.3%, calculated out of the entire *N*-glycome, $p < 0.05$, two-tailed paired student's t-test, day 0 vs. day 7), **Figure 2B**(VI)**, Table S20** and **Table S14A**. A significant lower expression of core fucosylation of day 7 macrophages (29.0% ± 5.4%) compared to day 0 monocytes (48.1% ± 3.4%) was also found when calculating the relative level of core fucosylation out of only the *N*-glycan types that are biosynthetically capable of receiving this type of modification ($p < 0.05$, two-tailed paired student's t-test, day 0 vs. day 7), **Table S20A**. The subtle *N*-glycome alterations were largely restricted to day 5-7 of the maturation process in accordance with the proteome-based segregation of the early (day 0-3) and late (day 5-7) maturation stages, **Figure S3**.
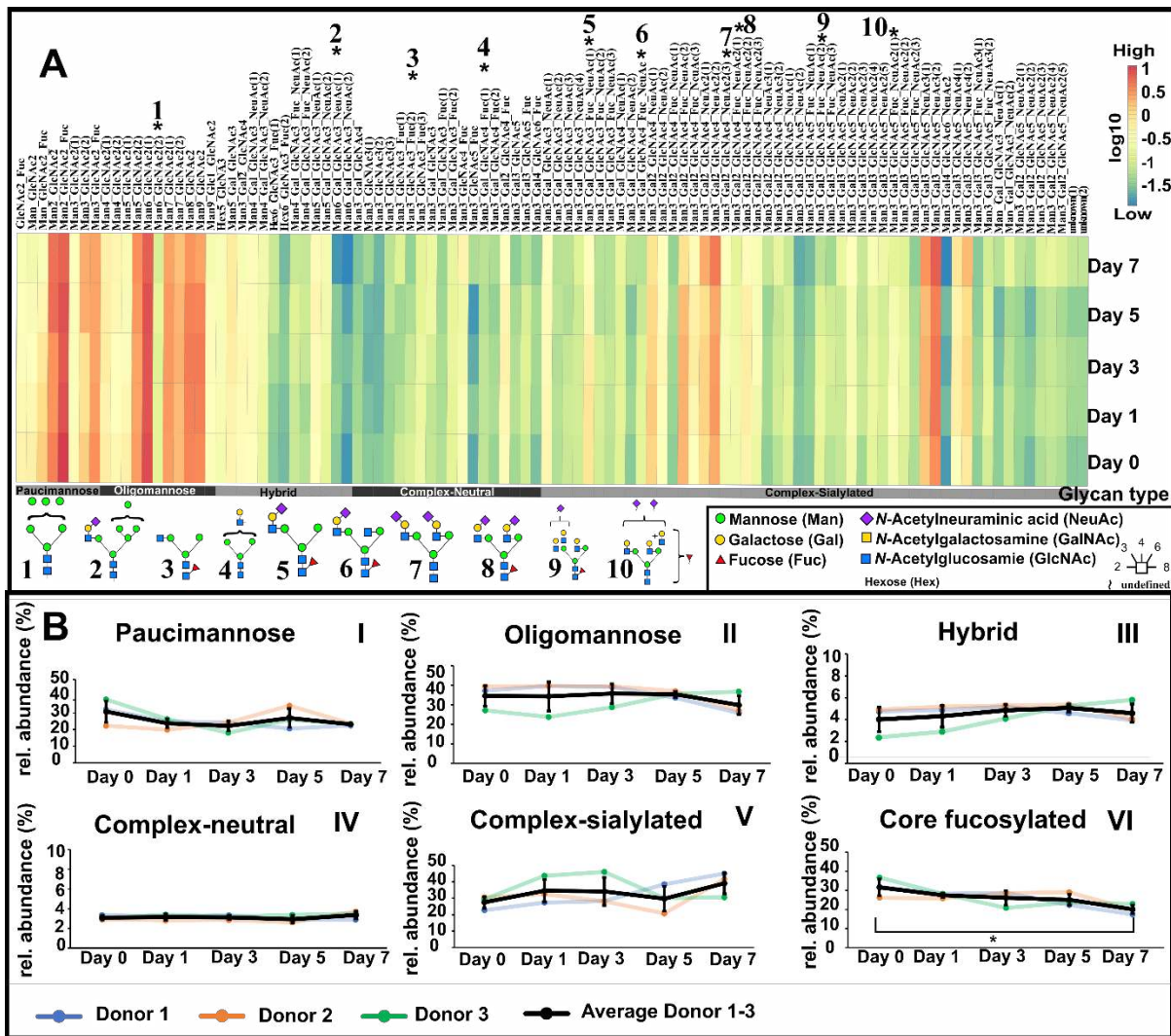
Figure 2. Longitudinal whole cell *N*-glycome profiling of maturing human macrophages. A) Heat map plotting the relative intensities (log$_{10}$ scale) of all identified 102 *N*-glycans over the seven-day macrophage maturation process. Note that the fine structures of the *N*-glycans, here represented as monosaccharide compositions due to space constraints, have been elucidated, see **Table S11**. *Only 10 *N*-glycan structures (consecutively numbered and depicted) showed significantly changed expression levels during maturation ($p < 0.05$, two-tailed paired student's t-test, day 0 vs. day 7, n = 3). **B**) Donor-specific longitudinal monitoring of the *N*-glycan types (I-V) and another abundant glycosylation feature i.e. core fucosylation (VI). These glycan features were calculated and plotted as a proportion of the total *N*-glycome. Black lines represent the average relative levels the three donors at each sampling point. *$p < 0.05$, two-tailed paired student's t-test, day 0 vs. day 7, n = 3. Data is plotted as mean ± SD.

Quantitative proteomics and glycopeptide analysis support a constitutively active truncation pathway

in monocytes and macrophages

Our glycomics data indicated constitutively high expression of paucimannosidic-type *N*-glycosylation in both monocytes (day 0: 30.8% ± 6.5%) and mature macrophages (day 7: 23.1% ± 0.5%). Paucimannosylation remains an under-reported and still debated type of protein *N*-glycosylation in human glycobiology (Loke, I., Kolarich, D., et al. 2016, Tjondro, H.C., Loke, I., et al. 2019). We and others have recently reported that this type of *N*-glycosylation is a prominent feature of neutrophil-mediated infection and immunity (Loke, I., Ostergaard, O., et al. 2017, Loke, I., Packer, N.H., et al. 2015, Thaysen-Andersen, M., Venkatakrishnan, V., et al. 2015), cancer (Becker, Y., Forster, S., et al. 2019, Chatterjee, S., Lee, L.Y., et al. 2019, Kaprio, T., Satomaa, T., et al. 2015, Sethi, M.K., Kim, H., et al. 2015) and cellular development (Dahmen, A.C., Fergen, M.T., et al. 2015), but so far not in primary monocyte-macrophage cell populations.

Consequently, we interrogated our proteomics data for intact glycopeptides to prove that the paucimannosidic-type *N*-glycans are in fact carried by human proteins commonly expressed by monocytes and macrophages. As exemplified by two intact *N*-glycopeptides identified with high confidence from HCD-MS/MS spectral evidence, paucimannosidic-type *N*-glycans, in particular, M2F were found to be carried by several anti-microbial monocyte-derived proteins including neutrophil elastase (P08246) and myeloperoxidase (P05164) (Kargi, H.A., Campbell, E.J., et al. 1990, Khan, A.A., Alsahli, M.A., et al. 2018, Nicholls, S.J. and Hazen, S.L. 2005), **Figure S5A-B**. Adding further support, these two immune-related glycoproteins were previously reported to carry paucimannosidic-type *N*-glycosylation signatures, in particular $Man_2GlcNAc_2Fuc_1$ (M2F), when studied from a neutrophil origin (Loke, I., Packer, N.H., et al. 2015, Ravnsborg, T., Houen, G., et al. 2010, Reiding, K.R., Franc, V., et al. 2019, Van Antwerpen, P., Slomianny, M.C., et al. 2010).

The quantitative proteomics data was then explored in order to assess the relative expression levels of the glycoside hydrolases putatively driving the truncation pathway responsible for the formation of

paucimannosidic proteins i.e. *N*-acetyl-β-hexosaminidase subunit α (P06865), *N*-acetyl-β-hexosaminidase subunit β (P07686) and lysosomal α-mannosidase (O00754) (Tjondro, H.C., Loke, I., et al. 2019). High and unaltered expression levels of these glycoside hydrolases over the entire seven-day macrophage maturation scheme were observed i.e. *N*-acetyl-β-hexosaminidase subunit α, day 0: $3.9 \times 10^8 \pm 7.6 \times 10^7$, day 1: $6.9 \times 10^8 \pm 5.9 \times 10^8$, day 3: $2.4 \times 10^8 \pm 6.1 \times 10^7$, day 5: $4.6 \times 10^8 \pm 7.6 \times 10^7$, day 7: $4.2 \times 10^8 \pm 5.9 \times 10^7$, *N*-acetyl-β-hexosaminidase subunit β, day 0: $1.4 \times 10^9 \pm 3.5 \times 10^8$, day 1: $9.6 \times 10^8 \pm 3.5 \times 10^8$, day 3: $1.3 \times 10^9 \pm 1.2 \times 10^8$, day 5: $1.3 \times 10^9 \pm 2.2 \times 10^8$, day 7: $1.4 \times 10^9 \pm 7.8 \times 10^7$), lysosomal α-mannosidase, day 0: $1.3 \times 10^9 \pm 7.5 \times 10^8$, day 1: $1.1 \times 10^9 \pm 7.5 \times 10^8$, day 3: $1.4 \times 10^9 \pm 2.6 \times 10^8$, day 5: $2.1 \times 10^9 \pm 4.1 \times 10^8$, day 7: $2.4 \times 10^9 \pm 3.8 \times 10^8$, all average ± SD protein intensity values, **Table S5-S6**. Thus, the quantitative proteomics data supports that the truncation pathway is constitutively active in both monocytes and macrophages providing a mechanistic explanation for the high levels of paucimannosidic proteins observed in these cell populations. The glycomics profile indicated a slightly reduced expression of paucimannosidic *N*-glycans during macrophage differentiation (day 0: 30.8% ± 6.5% vs. day 7: 23.1% ± 0.5%). This reduction, which did not reach statistical significance, may mechanistically be explained by a reduced protein level expression of the paucimannose-decorated proteases and other key glycoproteins predominantly expressed in monocytes rather than in macrophages i.e. neutrophil elastase, cathepsin G, and myeloperoxidase, **Figure S4,** as opposed to changes *per se* of the glycosylation enzymes catalysing the truncation pathway and the resulting *N*-glycan profile of these proteins, a hypothesis requiring further experimental testing.

Many other glycosylation enzymes involved in the formation or catabolism of *N*-glycoproteins were also identified and longitudinally monitored by the quantitative proteomics data including several other glycoside hydrolases i.e. β-galactosidase (P16278), tissue α-L-fucosidase (P04066), lysosomal α-glucosidase (P10253), α-galactosidase A (P06280), α-*N*-acetylglucosaminidase (P54802), Golgi α-mannosidase II (Q16706), glucosidase II subunit α (Q14697) and β (P14314), mannosyl-oligosaccharide glucosidase (MOGS, Q13724), and glycosyltransferases i.e. oligosaccharyl transferase subunit DAD1

(P61803) and UDP-glucose:glycoprotein glucosyltransferase 1 (Q9NYU2) as well as lectins involved in the glycoprotein synthesis and/or function i.e. IGF2R (P11717), galectin-1 (P09382), galectin-3 (P17931), galectin-9 (O00182), malectin (Q14165), C-type mannose receptor 2 (Q9UBG0), **Table S1.** With the exception of MOGS involved in the processing of the $Glc_3Man_9GlcNAc_2$ precursor after transfer to nascent glycoproteins, the expression of none of these biosynthetic enzymes and receptors were significantly altered during the macrophage maturation process (all $p \geq 0.05$, two-tailed paired student's t-test, day 0 vs. day 7) thereby providing some support for a relatively constant expression of the *N*-glycome during the monocyte-to-macrophage transition. However, it is important to note in this context that the human glycosylation machinery comprises more than 200 glycosylation enzymes (Nairn, A.V., Aoki, K., et al. 2012), and that many of the glyco-enzymes expressed at lower abundance were neither identified nor quantified in this study. Adding to this, Delannoy and colleagues have previously reported that the transcript level of several key glycosylation enzymes are in fact elevated upon differentiation of THP-1 macrophages including ST3GAL5, MGAT1, MGAT5, b4GALT1, FUT8 and NEU1 (Delannoy, C.P., Rombouts, Y., et al. 2017). Modulation of the glycosylation machinery during macrophage maturation was also suggested by other groups (Kohro, T., Tanaka, T., et al. 2004, Trottein, F., Schaffer, L., et al. 2009). Hence, dedicated studies using targeted or system-wide analysis of enzymes forming the glycosylation machinery either at the transcript level (i.e. quantitative PCR or RNASeq) or the protein level (i.e. parallel-reaction monitoring or data-dependent acquisition proteomics) are required to fully understand how the glycosylation machinery is affected during the maturation of primary macrophages.

Lectin flow cytometry indicates cell surface glycan remodelling upon macrophage maturation

To complement the whole cell glycomics data, we performed cell surface analysis of the glycoepitope expression of the maturing CD14^{+}-monocytes using lectin flow cytometry employing ConA and WGA, two plant lectins displaying a known reactivity for branched α-mannosyl-epitopes exclusively found in

N-glycans and β-GlcNAc-/α-NeuAc-epitopes, respectively, **Figure 3**. Strong cell surface reactivity of both lectins, significantly above the background fluorescence of unstained cells, was observed for the monocyte-macrophage cell populations. Interestingly, differentiation of monocytes into macrophages was accompanied by a significant increase in ConA binding to mature macrophages on day 7. Attempts to perform lectin flow cytometry using Mannitou-IgM, an antibody known to recognise paucimannosidic epitopes (Becker, Y., Forster, S., et al. 2019), to probe for a cell surface presentation of paucimannosidic proteins were hampered by significant clumping/aggregation of cells as a likely result of the multi-valent binding properties of IgM (data not shown). The basis for the elevated ConA reactivity in day 7 macrophages therefore remains unclear. Future lectin flow cytometry experiments using Mannitou-IgG or plant lectins able to discriminate between the various classes of mannose-terminating glycoconjugates and possibly complemented with the use of subcellular fractionation techniques or cell surface capture technologies followed by LC-MS/MS-based glycomics are required to fully delineate the relative contribution of the oligomannosidic and paucimannosidic proteins to the intriguing ConA reactivity to the cell surfaces of mature macrophages as well as the intracellular distribution of these glycoproteins.

Further, a progressive increase in the WGA reactivity was observed during macrophage differentiation, reaching significance only at day 5, when compared to undifferentiated monocytes (day 0 and 1). The quantitative whole cell glycomics data revealed that a significant proportion of the monocyte-macrophage *N*-glycome comprises α2,3-/α2,6-sialylated complex-type *N*-glycans (27.6%-39.1%) and that six of the ten *N*-glycan structures showing changed expression levels during maturation were in fact capped by sialic acid residues (Figure 2A). Such mature sialylated *N*-glycans, as well as the highly sialylated *O*-glycans (discussed below), are most likely present on the cell surface and would thus contribute significantly to the observed WGA signal in the lectin flow cytometry data. It remains unexplored if the elevated WGA reactivity at day 5 is a result of an enhanced cell surface presentation of α2,3- and/or α2,6-sialylated *N*- and *O*-glycan structures by cell surface proteins (or alternatively by cell surface glycosphingolipids), aspects that could be investigated before and after

sialidase treatment using other plant lectins that recognise these glycoepitopes including SNA, MAL-I and MAL-II.

Considering the importance of the cell surface localised glycoepitopes for immune cell communication and the significant glycan remodelling indicated here to be associated with monocyte-macrophage differentiation, future studies focusing on delineating the temporal-spatial presentation of glycans on the surface during maturation of monocytes with fine structure resolution and efforts attempting to understand the mechanisms that drive such glycan remodelling are clearly warranted.
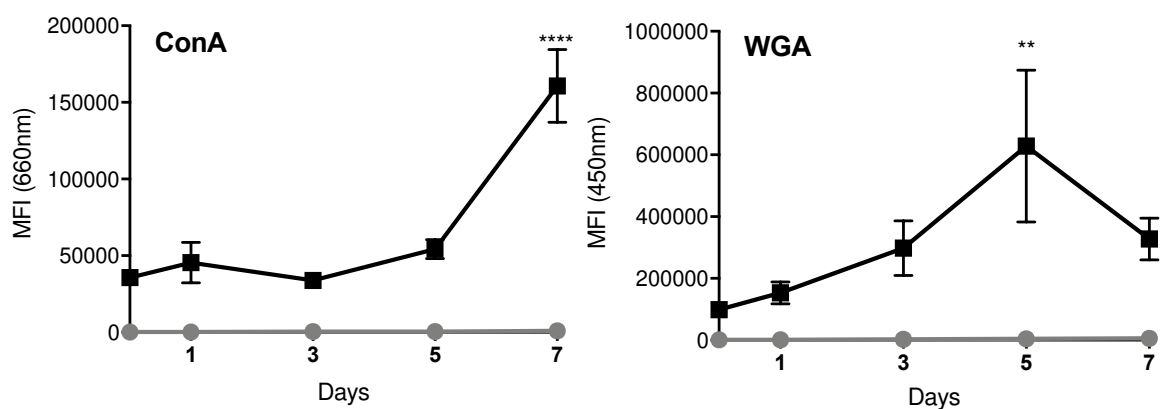

Figure 3. The presentation of cell surface glycoepitopes on differentiating human CD14^{+}-monocytes was assessed by WGA and ConA-based lectin flow cytometry (black lines). The signals from unstained cells are represented by grey lines. A significant increase in the ConA reactivity was observed at day 7 compared to all other time points, and in the WGA reactivity at day 5 compared to undifferentiated monocytes at day 0 and day 1. MFI, mean fluorescence intensity. Data is plotted as the mean and standard error of measurements of cells obtained from three donors. ** $p < 0.01$, **** $p < 0.0001$ by two-way ANOVA.

Subtle O-glycome changes during macrophage differentiation

The *O*-glycomics data allowed profiling of a total of 15 glycans comprising mainly unsubstituted core 1- and 2-type *O*-glycans and a few sulfated structures identified at relatively low abundance, **Figure**

4A and **Table S21-S23**. Annotated spectral data is available documenting the structural details of the reported *O*-glycans, see **Supplementary data 1**. Quantitative profiling demonstrated that only a single *O*-glycan was significantly altered over the time course i.e. the high abundance $Gal_2GlcNAc_1GalNAc_1NeuAc_2$ showed reduced expression with progressive macrophage transition in particular during the late stage maturation ($p < 0.05$, two-tailed paired student's t-test, day 0 vs. day 7), **Figure 4B** (Structure 4) and **Table S22-S27**. In support of our findings, Bax and colleagues identified the same *O*-glycan signatures and reported $Hex_1HexNAc_1NeuAc_1$ (presumably $Gal_1GalNAc_1NeuAc_1$) as the most abundant structure of maturing human $CD14^+$-monocytes (resembling our day 5 cells) using MALDI-TOF-MS/MS profiling and interestingly also reported a decrease of core 2-type *O*-glycans during GM-CSF-mediated differentiation of human $CD14^+$-monocytes to dendritic cells (Bax, M., García-Vallejo, J.J., et al. 2007). By grouping the observed *O*-glycan structures according to their core types, we found that both core 1- and core 2-type *O*-glycans were significantly altered in expression during macrophage differentiation ($p = 0.048$, up-regulation and $p = 0.048$ down-regulation, respectively, two-tailed paired student's t-test, day 0 vs. day 7), which collectively generated a substantial difference in the core 1-core 2 *O*-glycan ratio from day 0 (6.4) relative to day 7 (12.4) cells, **Table S22A**. Conversely, the level of *O*-glycan sialylation remained largely unchanged over the differentiation course i.e. day 0 (2.5%:62.4%:35.1%) and day 7 (1.1%:65.6%:33.3%) (written as the average relative proportion of asialo:monosialo:diasialo-*O*-glycans), demonstrating that the lower level of the disialylated core 2-type *O*-glycan observed at day 7 arises from a general shift towards the core 1-type *O*-glycosylation rather than a reduced *O*-glycan sialylation in day 7 macrophages relative to day 0 monocytes. These subtle alterations in the relative distribution of the observed *O*-glycans have been plotted on the well-established *O*-glycosylation biosynthetic pathway, **Figure S6** (Kudelka, M.R., Ju, T., et al. 2015). Importantly, several intact core 1- and core 2-type *O*-glycopeptides from human glycoproteins of monocyte-macrophage origin including the macrophage mannose receptor 1 (UniProtKB, P22897) were identified in the proteomics data providing support for the *O*-glycomics data, **Figure S5C-D**.

Taken together, these observations indicate that the biosynthetic pathways for *O*-glycoproteins are altered in subtle ways during macrophage maturation, a hypothesis we unfortunately were unable to confirm using our proteomics data sets. The proteomics experiments only detected a few glycosylation enzymes involved in *O*-glycoprotein biosynthesis and catabolism, which all showed a stable expression across the differentiation period, including α-*N*-acetylgalactosaminidase (P17050), polypeptide *N*-acetylgalactosaminyltransferase (Q10471), GDP-fucose protein *O*-fucosyltransferase (Q9H488) and carbohydrate sulfotransferase (Q9NPF2) (data not shown). The glycosylation enzymes directly involved in core 1- and core 2-type *O*-glycoprotein synthesis, the abundant *O*-glycan features observed in the monocyte-macrophage *O*-glycome, e.g. core 2/core 4 beta-1,6-*N*-acetylglucosaminyltransferase (O95395) were unfortunately not identified in the proteomics experiments.
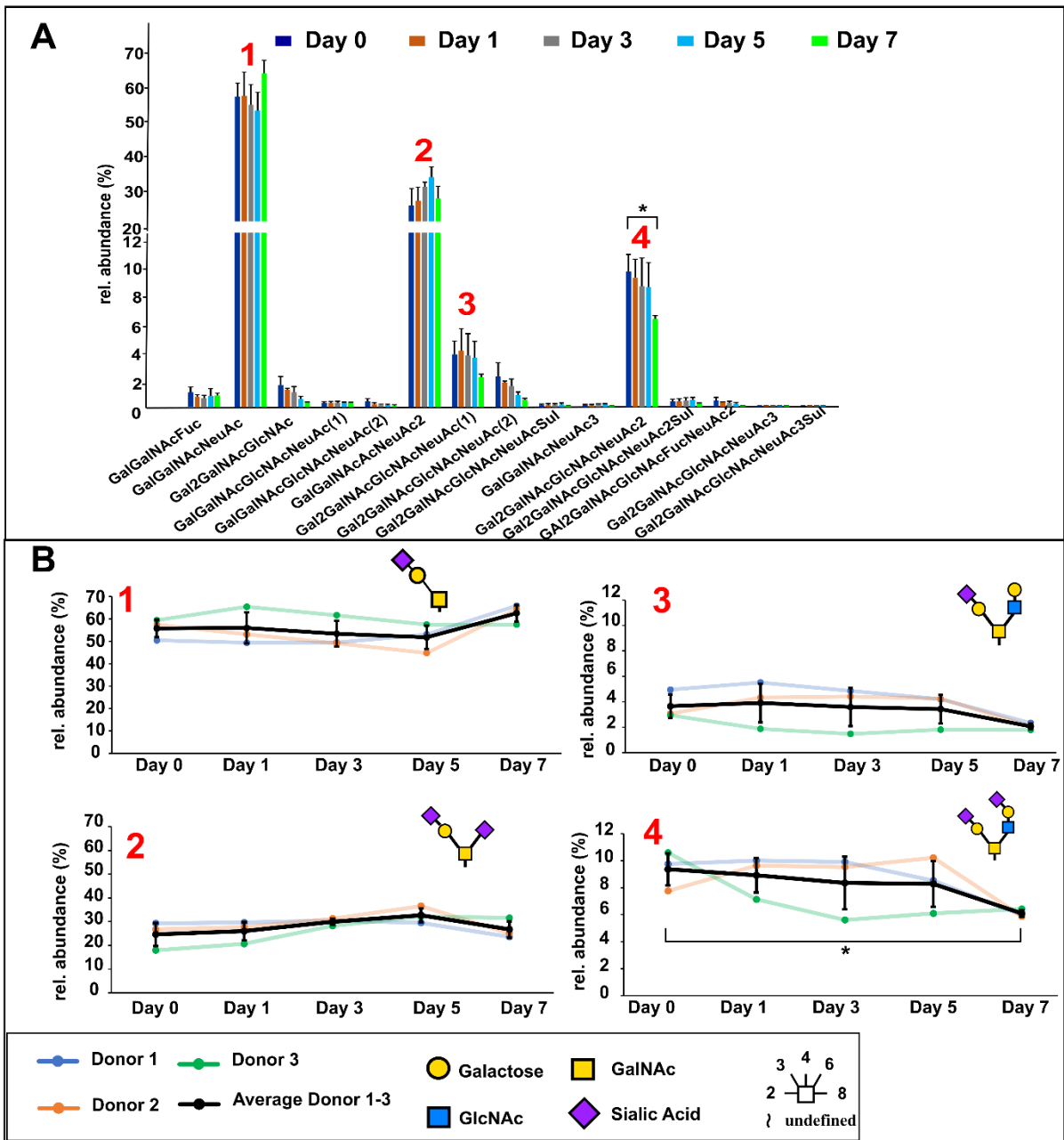
Figure 4. Longitudinal *O*-glycome profiling of maturing human macrophages. **A**) Relative abundance of the identified *O*-glycans over the seven-day differentiation process. Data is plotted as mean ± SD, n = 3. *p < 0.05, two-tailed paired student's t-test (day 0 vs. day 7). Sul: Sulfate. **B**) Donor-specific longitudinal monitoring of four abundant *O*-glycan structures (Structure 1-4, also indicated in panel A). The black lines represent the average of three donors at each sampling point. Data points are plotted as mean ± SD, n = 3. *p < 0.05, two-tailed paired student's t-test (day 0 vs. day 7).

Biological importance and individual-specific glycome variation of human monocyte-macrophages

Complex carbohydrates carried by intra- and extracellular glycoproteins are recognised by a spectrum of glycan-binding proteins including endogenous lectins and microbial adhesins that concertedly mediate and modulate diverse functions within the diverse cell types of the innate immune system not least monocytes and macrophages (Baum, L.G. and Cobb, B.A. 2017, Schnaar, R.L. 2016, Zhou, J.Y., Oswald, D.M., et al. 2018). Given their distinct functions *in vivo* and highly different tissue environments (Murray, P.J. 2017), we herein set out to document the *N*- and *O*-glycosylation features expressed by monocytes and macrophages expecting that the profiling would reveal distinct glycome expression patterns despite the cellular relatedness between these two cell types. Forming the basis of this hypothesis, *O*-glycan remodelling during B cell differentiation (Giovannone, N., Antonopoulos, A., et al. 2018), *N*- and *O*-glycosylation alterations during *in vitro* differentiation of THP-1 monocytes to macrophage-like cells (Delannoy, C.P., Rombouts, Y., et al. 2017), and glycosylation differences between immature monocyte-derived dendritic cells and their mature counterpart (Bax, M., García-Vallejo, J.J., et al. 2007) have previously been reported.

Thus, our quantitative whole cell glycomics data presented in this study indicating relative stable expression of the cellular protein *N*- and *O*-glycome during macrophage maturation may, on the face of it, appear surprising given the known dynamics and physiology-dependent nature of the mammalian glycosylation machinery (Moremen, K.W., Tiemeyer, M., et al. 2012). Mature macrophages may, however, still, in effect, display a unique glycosylation phenotype that is distinctly different from their monocytic precursors by manipulating the glycoproteome and/or alter the spatial arrangement of the expressed glycome, details not presently captured by conventional whole cell glycomics experiments. Our proteomics data in fact indicated a maturation stage-dependent proteome expression that corroborated other proteomics literature produced from monocyte-macrophage cell populations indicating strong protein level regulation during macrophage maturation. Dynamic temporal-spatial presentation of glycans on the cell surface without necessarily

changing the glyco(proteo)me expression is also a recognised mechanism used by cells to alter their "glycan-code" (Moremen, K.W., Tiemeyer, M., et al. 2012). Our observation of a highly increased ConA reactivity to mature macrophages (day 7) using lectin flow cytometry despite a concomitant reduction in the expression of mannose-terminating *N*-glycans within the cellular *N*-glycome may represent an example of temporal-spatial glycan "remodelling". The mannose-rich glycoepitope expression patterns on the surfaces of mature macrophages may be particularly interesting given the diverse repertoire of mannose-recognising lectins displaying both endocytic and signalling capacity including the macrophage mannose receptor 1 (P22897) and C-type mannose receptor 2 (Q9UBG0) (Loke, I., Kolarich, D., et al. 2016). The identity and involvement of these surface-located manno-conjugates in the diverse functions carried out by monocytes and macrophages require further exploration. It should also be pointed out that other glycoconjugate classes not profiled in this study including glycosphingolipids (e.g. GM3) and *O*-mannose and *O*-GlcNAc-type modifications as well as the various classes of proteoglycans and glycosaminoglycans may contribute to the glycan remodelling underpinning the monocyte-to-macrophage transition and may therefore be important glycosylation features defining the "glycosylation phenotype" pertaining to monocytes and macrophages, aspects that require dedicated follow-up studies using tailored analytical approaches.

Noteworthy, relatively large donor-to-donor glycome and proteome variations were observed throughout this profiling study possibly reflecting a considerable physiology-dependent or inherited heterogeneity of the isolated CD14^{+}-monocyte populations used for analysis in this study, and, further, indicates that multiple macrophage differentiation pathways may exist. Pronounced cellular and molecular heterogeneity may represent a general feature of stem and progenitor cells harbouring differentiation potential, and may thus be a feature also of other immune and non-immune cell types (Corfield, A.P. and Berry, M. 2015, Tarique, A.A., Logan, J., et al. 2015). Notably, the inter-donor variation was pronounced in the undifferentiated CD14^{+}-monocytes and in the early-/mid-stage maturation process while convergence of the molecular heterogeneity was observed at the maturation end point (day 7), see examples of protein convergence in Figure S2 and Figure S4 and

glycan convergence in Figure 4B. Given the significant inter-donor variation reported herein, experimental designs using longitudinal measurements of monocyte-macrophage populations from the same donor rather than comparing cell populations between donors appears to be a more informative approach. Follow-up studies using a larger cohort of healthy donors and/or repeat sampling from the same set of individuals are required to further explore this intriguing biological variation and to determine if the GM-CSF-mediated *ex vivo* convergence of macrophages observed in this study is reflected in macrophage populations *in vivo*, for example from macrophage-rich atherosclerotic plaques or alveolar or hepatic macrophages obtained from patients undergoing lung or liver transplantation or lobectomy. Further, characterisation of macrophage subpopulations and associated changes in glycoimmunological traits during strong pro- and anti-inflammatory stimulation (M1- and M2-macrophage polarisation, respectively) should also be subjected to future investigations.

In conclusion, this high-resolution system-wide map of the protein *N*- and *O*-glycome associated with healthy monocyte-to-macrophage transition, the most detailed to date, aids our understanding of the molecular makeup of two important types of innate immune cells and forms an essential point of reference for future glycoimmunological studies involving human monocytes and macrophages.

34

Abbreviations

ACN: acetonitrile; AGC: automatic gain control; CID: collision-induced dissociation; FBS: foetal bovine serum; FA: formic acid; Fuc: fucose/fucosyl; Gal: galactose/galactosyl; GalNAc, *N*-acetylgalactosamine/*N*-acetylgalactosaminyl; GlcNAc: *N*-acetylglucosamine/*N*-acetylglucosaminyl; GM-CSF: granulocyte-macrophage colony-stimulating factor; HCD: higher-energy collisional dissociation; MALDI-TOF: matrix-assisted laser desorption/ionisation-time-of-flight; Man: mannose/mannosyl; NeuAc: *N*-acetylneuraminic acid; PGC-LC-MS/MS: porous graphitised carbon-liquid chromatography-tandem mass spectrometry; SPE: solid-phase extraction; Sul: sulfate; TEAB: triethylammonium bicarbonate; TLR: Toll-like receptor; WGA: wheat germ agglutinin.

References

Abrahams JL, Campbell MP, Packer NH. 2018. Building a PGC-LC-MS N-glycan retention library and elution mapping resource. *Glycoconjugate journal*, 35:15-29.

Abrahams JL, Packer NH, Campbell MP. 2015. Relative quantitation of multi-antennary N-glycan classes: combining PGC-LC-ESI-MS with exoglycosidase digestion. *Analyst*, 140:5444-5449.

Aebi M. 2013. N-linked protein glycosylation in the ER. *Biochimica et biophysica acta*, 1833:2430-2437.

Ashwood C, Lin CH, Thaysen-Andersen M, Packer NH. 2018. Discrimination of Isomers of Released N- and O-Glycans Using Diagnostic Product Ions in Negative Ion PGC-LC-ESI-MS/MS. *Journal of the American Society for Mass Spectrometry*, 29:1194-1209.

Baum LG, Cobb BA. 2017. The direct and indirect effects of glycans on immune function. *Glycobiology*, 27:619-624.

Bax M, García-Vallejo JJ, Jang-Lee J, North SJ, Gilmartin TJ, Hernández G, Crocker PR, Leffler H, Head SR, Haslam SM*, et al.* 2007. Dendritic Cell Maturation Results in Pronounced Changes in Glycan Expression Affecting Recognition by Siglecs and Galectins. *The Journal of Immunology*, 179:8216-8224.

Becker Y, Forster S, Gielen GH, Loke I, Thaysen-Andersen M, Laurini C, Wehrand K, Pietsch T, Diestel S. 2019. Paucimannosidic glycoepitopes inhibit tumorigenic processes in glioblastoma multiforme. *Oncotarget*, 10:4449-4465.

Benjamini YaH, Y. 1995. Controlling the false discovery rate: A Practical and powerful approach to multiple testing. *J. Roy. Statist. Soc.*, 57:289-300.

Berger RP, Dookwah M, Steet R, Dalton S. 2016. Glycosylation and stem cells: Regulatory roles and application of iPSCs in the study of glycosylation-related disorders. *BioEssays : news and reviews in molecular, cellular and developmental biology*, 38:1255-1265.

Cerliani JP, Blidner AG, Toscano MA, Croci DO, Rabinovich GA. 2017. Translating the 'Sugar Code' into Immune and Vascular Signaling Programs. *Trends in Biochemical Sciences*, 42:255-273.

Chatterjee S, Lee LY, Kawahara R, Abrahams JL, Adamczyk B, Anugraham M, Ashwood C, Sumer-Bayraktar Z, Briggs MT, Chik JHL*, et al.* 2019. Protein Paucimannosylation is an Enriched N-glycosylation Signature of Human Cancers. *Proteomics*:e1900010.

Clark MC, Baum LG. 2012. T cells modulate glycans on CD43 and CD45 during development and activation, signal regulation, and survival. *Annals of the New York Academy of Sciences*, 1253:58-67.

Corfield AP, Berry M. 2015. Glycan variation and evolution in the eukaryotes. *Trends Biochem Sci*, 40:351-359.

Court M, Petre G, Atifi ME, Millet A. 2017. Proteomic Signature Reveals Modulation of Human Macrophage Polarization and Functions Under Differing Environmental Oxygen Conditions. *Molecular & cellular proteomics : MCP*, 16:2153-2168.

Cox J, Mann M. 2008. MaxQuant enables high peptide identification rates, individualized p.p.b.-range mass accuracies and proteome-wide protein quantification. *Nat Biotechnol*, 26:1367-1372.

Dahmen AC, Fergen MT, Laurini C, Schmitz B, Loke I, Thaysen-Andersen M, Diestel S. 2015. Paucimannosidic glycoepitopes are functionally involved in proliferation of neural progenitor cells in the subventricular zone. *Glycobiology*, 25:869-880.

Delannoy CP, Rombouts Y, Groux-Degroote S, Holst S, Coddeville B, Harduin-Lepers A, Wuhrer M, Elass-Rochard E, Guerardel Y. 2017. Glycosylation Changes Triggered by the Differentiation of Monocytic THP-1 Cell Line into Macrophages. *Journal of proteome research*, 16:156-169.

Eligini S, Brioschi M, Fiorelli S, Tremoli E, Banfi C, Colli S. 2015. Human monocyte-derived macrophages are heterogenous: Proteomic profile of different phenotypes. *Journal of proteomics*, 124:112-123.

Everest-Dass AV, Jin D, Thaysen-Andersen M, Nevalainen H, Kolarich D, Packer NH. 2012. Comparative structural analysis of the glycosylation of salivary and buccal cell proteins: innate protection against infection by Candida albicans. *Glycobiology*, 22:1465-1479.

Geissmann F, Manz MG, Jung S, Sieweke MH, Merad M, Ley K. 2010. Development of monocytes, macrophages, and dendritic cells. *Science (New York, N.Y.)*, 327:656-661.

Giovannone N, Antonopoulos A, Liang J, Geddes Sweeney J, Kudelka MR, King SL, Lee GS, Cummings RD, Dell A, Barthel SR*, et al.* 2018. Human B Cell Differentiation Is Characterized by Progressive Remodeling of O-Linked Glycans. *Frontiers in Immunology*, 9.

Gleissner C. 2012. Macrophage Phenotype Modulation by CXCL4 in Atherosclerosis. *Frontiers in Physiology*, 3.

Gonzalez-Mejia ME, Doseff AI. 2009. Regulation of monocytes and macrophages cell fate. *Frontiers in bioscience (Landmark edition)*, 14:2413-2431.

Hare NJ, Lee LY, Loke I, Britton WJ, Saunders BM, Thaysen-Andersen M. 2017. Mycobacterium tuberculosis Infection Manipulates the Glycosylation Machinery and the N-Glycoproteome of Human Macrophages and Their Microparticles. *J Proteome Res*, 16:247-263.

Harvey DJ. 2005a. Fragmentation of negative ions from carbohydrates: part 2. Fragmentation of high-mannose N-linked glycans. *Journal of the American Society for Mass Spectrometry*, 16:631-646.

Harvey DJ. 2005b. Fragmentation of negative ions from carbohydrates: part 3. Fragmentation of hybrid and complex N-linked glycans. *Journal of the American Society for Mass Spectrometry*, 16:647-659.

Hinneburg H, Chatterjee S, Schirmeister F, Nguyen-Khuong T, Packer NH, Rapp E, Thaysen-Andersen M. 2019. Post-Column Make-up Flow (PCMF) Enhances the Performance of Capillary-Flow PGC-LC-MS/MS-Based Glycomics. *Analytical chemistry*.

Hirayama D, Iida T, Nakase H. 2017. The Phagocytic Function of Macrophage-Enforcing Innate Immunity and Tissue Homeostasis. *International journal of molecular sciences*, 19.

Huang da W, Sherman BT, Lempicki RA. 2009. Bioinformatics enrichment tools: paths toward the comprehensive functional analysis of large gene lists. *Nucleic acids research*, 37:1-13.

Italiani P, Boraschi D. 2014. From Monocytes to M1/M2 Macrophages: Phenotypical vs. Functional Differentiation. *Frontiers in Immunology*, 5.

Jakubzick CV, Randolph GJ, Henson PM. 2017. Monocyte differentiation and antigen-presenting functions. *Nature reviews. Immunology*, 17:349-362.

Jensen PH, Karlsson NG, Kolarich D, Packer NH. 2012. Structural analysis of N- and O-glycans released from glycoproteins. *Nature protocols*, 7:1299-1310.

Kaprio T, Satomaa T, Heiskanen A, Hokke CH, Deelder AM, Mustonen H, Hagstrom J, Carpen O, Saarinen J, Haglund C. 2015. N-glycomic profiling as a tool to separate rectal adenomas from carcinomas. *Mol Cell Proteomics*, 14:277-288.

Kargi HA, Campbell EJ, Kuhn C, 3rd. 1990. Elastase and cathepsin G of human monocytes: heterogeneity and subcellular localization to peroxidase-positive granules. *The journal of histochemistry and cytochemistry : official journal of the Histochemistry Society*, 38:1179-1186.

Khan AA, Alsahli MA, Rahmani AH. 2018. Myeloperoxidase as an Active Disease Biomarker: Recent Biochemical and Pathological Perspectives. *Medical sciences (Basel, Switzerland)*, 6.

Kohro T, Tanaka T, Murakami T, Wada Y, Aburatani H, Hamakubo T, Kodama T. 2004. A comparison of differences in the gene expression profiles of phorbol 12-myristate 13-acetate differentiated THP-1 cells and human monocyte-derived macrophage. *J Atheroscler Thromb*, 11:88-97.

Kraft-Terry SD, Gendelman HE. 2011. Proteomic biosignatures for monocyte-macrophage differentiation. *Cellular immunology*, 271:239-255.

Kudelka MR, Ju T, Heimburg-Molinaro J, Cummings RD. 2015. Simple sugars to complex disease--mucin-type O-glycans in cancer. *Adv Cancer Res*, 126:53-135.

Lau KS, Partridge EA, Grigorian A, Silvescu CI, Reinhold VN, Demetriou M, Dennis JW. 2007. Complex N-Glycan Number and Degree of Branching Cooperate to Regulate Cell Proliferation and Differentiation. *Cell*, 129:123-134.

Lee LY, Moh ES, Parker BL, Bern M, Packer NH, Thaysen-Andersen M. 2016. Toward Automated N-Glycopeptide Identification in Glycoproteomics. *Journal of proteome research*, 15:3904-3915.

Loke I, Kolarich D, Packer NH, Thaysen-Andersen M. 2016. Emerging roles of protein mannosylation in inflammation and infection. *Mol Aspects Med*, 51:31-55.

Loke I, Ostergaard O, Heegaard NHH, Packer NH, Thaysen-Andersen M. 2017. Paucimannose-Rich N-glycosylation of Spatiotemporally Regulated Human Neutrophil Elastase Modulates Its Immune Functions. *Mol Cell Proteomics*, 16:1507-1527.

Loke I, Packer NH, Thaysen-Andersen M. 2015. Complementary LC-MS/MS-Based N-Glycan, N-Glycopeptide, and Intact N-Glycoprotein Profiling Reveals Unconventional Asn71-Glycosylation of Human Neutrophil Cathepsin G. *Biomolecules*, 5:1832-1854.

Lyons JJ, Milner JD, Rosenzweig SD. 2015. Glycans Instructing Immunity: The Emerging Role of Altered Glycosylation in Clinical Immunology. *Frontiers in Pediatrics*, 3.

Martinez FO, Gordon S, Locati M, Mantovani A. 2006. Transcriptional profiling of the human monocyte-to-macrophage differentiation and polarization: new molecules and patterns of gene expression. *Journal of immunology (Baltimore, Md. : 1950)*, 177:7303-7311.

Martinez FO, Sica A, Mantovani A, Locati M. 2008. Macrophage activation and polarization. *Frontiers in bioscience : a journal and virtual library*, 13:453-461.

Mills CD, Kincaid K, Alt JM, Heilman MJ, Hill AM. 2000. M-1/M-2 macrophages and the Th1/Th2 paradigm. *Journal of immunology (Baltimore, Md. : 1950)*, 164:6166-6173.

Moremen KW, Tiemeyer M, Nairn AV. 2012. Vertebrate protein glycosylation: diversity, synthesis and function. *Nature reviews. Molecular cell biology*, 13:448-462.

Murray PJ. 2017. Macrophage Polarization. *Annual review of physiology*, 79:541-566.

Nairn AV, Aoki K, dela Rosa M, Porterfield M, Lim JM, Kulik M, Pierce JM, Wells L, Dalton S, Tiemeyer M*, et al.* 2012. Regulation of glycan structures in murine embryonic stem cells: combined transcript profiling of glycan-related genes and glycan structural analysis. *J Biol Chem*, 287:37835-37856.

Nicholls SJ, Hazen SL. 2005. Myeloperoxidase and cardiovascular disease. *Arterioscler Thromb Vasc Biol*, 25:1102-1111.

Nonaka M, Ma BY, Murai R, Nakamura N, Baba M, Kawasaki N, Hodohara K, Asano S, Kawasaki T. 2008. Glycosylation-dependent interactions of C-type lectin DC-SIGN with colorectal tumor-associated Lewis glycans impair the function and differentiation of monocyte-derived dendritic cells. *Journal of immunology (Baltimore, Md. : 1950)*, 180:3347-3356.

Ohtsubo K, Marth JD. 2006. Glycosylation in cellular mechanisms of health and disease. *Cell*, 126:855-867.

Pabst M, Altmann F. 2008. Influence of electrosorption, solvent, temperature, and ion polarity on the performance of LC-ESI-MS using graphitic carbon for acidic oligosaccharides. *Analytical chemistry*, 80:7534-7542.

Palmisano G, Larsen MR, Packer NH, Thaysen-Andersen M. 2013. Structural analysis of glycoprotein sialylation – part II: LC-MS based detection. *RSC Advances*, 3:22706-22726.

Queval CJ, Brosch R, Simeone R. 2017. The Macrophage: A Disputed Fortress in the Battle against Mycobacterium tuberculosis. *Frontiers in Microbiology*, 8.

Ravnsborg T, Houen G, Hojrup P. 2010. The glycosylation of myeloperoxidase. *Biochim Biophys Acta*, 1804:2046-2053.

Reiding KR, Franc V, Huitema MG, Brouwer E, Heeringa P, Heck AJR. 2019. Neutrophil myeloperoxidase harbors distinct site-specific peculiarities in its glycosylation. *J Biol Chem*.

Sander J, Schmidt SV, Cirovic B, McGovern N, Papantonopoulou O, Hardt AL, Aschenbrenner AC, Kreer C, Quast T, Xu AM*, et al.* 2017. Cellular Differentiation of Human Monocytes Is Regulated by Time-Dependent Interleukin-4 Signaling and the Transcriptional Regulator NCOR2. *Immunity*, 47:1051-1066.e1012.

Schnaar RL. 2016. Glycobiology simplified: diverse roles of glycan recognition in inflammation. *J Leukoc Biol*, 99:825-838.

Sethi MK, Kim H, Park CK, Baker MS, Paik YK, Packer NH, Hancock WS, Fanayan S, Thaysen-Andersen M. 2015. In-depth N-glycome profiling of paired colorectal cancer and non-tumorigenic tissues reveals cancer-, stage- and EGFR-specific protein N-glycosylation. *Glycobiology*, 25:1064-1078.

Springer SA, Gagneux P. 2016. Glycomics: revealing the dynamic ecology and evolution of sugar molecules. *Journal of proteomics*, 135:90-100.

Tarique AA, Logan J, Thomas E, Holt PG, Sly PD, Fantino E. 2015. Phenotypic, functional, and plasticity features of classical and alternatively activated human macrophages. *American journal of respiratory cell and molecular biology*, 53:676-688.

Tedla N, Glaros EN, Brunk UT, Jessup W, Garner B. 2004. Heterogeneous expression of apolipoprotein-E by human macrophages. *Immunology*, 113:338-347.

Thaysen-Andersen M, Mysling S, Højrup P. 2009. Site-Specific Glycoprofiling of N-Linked Glycopeptides Using MALDI-TOF MS: Strong Correlation between Signal Strength and Glycoform Quantities. *Analytical chemistry*, 81:3933-3943.

Thaysen-Andersen M, Venkatakrishnan V, Loke I, Laurini C, Diestel S, Parker BL, Packer NH. 2015. Human neutrophils secrete bioactive paucimannosidic proteins from azurophilic granules into pathogen-infected sputum. *J Biol Chem*, 290:8789-8802.

Tjondro HC, Loke I, Chatterjee S, Thaysen-Andersen M. 2019. Human protein paucimannosylation: cues from the eukaryotic kingdoms. *Biol Rev Camb Philos Soc*.

Trombetta ES. 2003. The contribution of N-glycans and their processing in the endoplasmic reticulum to glycoprotein biosynthesis. *Glycobiology*, 13:77r-91r.

Trottein F, Schaffer L, Ivanov S, Paget C, Vendeville C, Cazet A, Groux-Degroote S, Lee S, Krzewinski-Recchi MA, Faveeuw C*, et al.* 2009. Glycosyltransferase and sulfotransferase gene expression profiles in human monocytes, dendritic cells and macrophages. *Glycoconjugate journal*, 26:1259-1274.

Van Antwerpen P, Slomianny MC, Boudjeltia KZ, Delporte C, Faid V, Calay D, Rousseau A, Moguilevsky N, Raes M, Vanhamme L*, et al.* 2010. Glycosylation pattern of mature dimeric leukocyte and recombinant monomeric myeloperoxidase: glycosylation is required for optimal enzymatic activity. *J Biol Chem*, 285:16351-16359.

van Kooyk Y, Rabinovich GA. 2008. Protein-glycan interactions in the control of innate and adaptive immune responses. *Nature immunology*, 9:593-601.

Varki A. 2016. Biological roles of glycans. *Glycobiology*, 27:3-49.

Varki A CR, Esko JD, et al., editors. . 2015-2017. Essentials of Glycobiology [Internet]. 3rd edition. https://www.ncbi.nlm.nih.gov/books/NBK310274/. *Cold Spring Harbor (NY): Cold Spring Harbor Laboratory Press*.

Varki A, Cummings RD, Aebi M, Packer NH, Seeberger PH, Esko JD, Stanley P, Hart G, Darvill A, Kinoshita T, *et al.* 2015. Symbol Nomenclature for Graphical Representations of Glycans. *Glycobiology*, 25:1323-1324.

Walters SB, Kieckbusch J, Nagalingam G, Swain A, Latham SL, Grau GER, Britton WJ, Combes V, Saunders BM. 2013. Microparticles from Mycobacteria-Infected Macrophages Promote Inflammation and Cellular Migration. *The Journal of Immunology*, 190:669-677.

Wessel D, Flugge UI. 1984. A method for the quantitative recovery of protein in dilute solution in the presence of detergents and lipids. *Analytical biochemistry*, 138:141-143.

Zarif JC, Yang W, Hernandez JR, Zhang H, Pienta KJ. 2017. The Identification of Macrophage-enriched Glycoproteins Using Glycoproteomics. *Molecular & cellular proteomics : MCP*, 16:1029-1037.

Zhang WY, Gaynor PM, Kruth HS. 1996. Apolipoprotein E produced by human monocyte-derived macrophages mediates cholesterol efflux that occurs in the absence of added cholesterol acceptors. *The Journal of biological chemistry*, 271:28641-28646.

Zhou JY, Oswald DM, Oliva KD, Kreisman LSC, Cobb BA. 2018. The Glycoscience of Immunity. *Trends Immunol*, 39:523-535.